Journal of Power Sources 199 (2012) 336–340

Contents lists available at SciVerse ScienceDirect

Journal of Power Sources

journal homepage: www.elsevier.com/locate/jpowsour

Short communication

A new electrochemical reaction mechanism of tin pyrophosphate thin film with lithium

Qin-Qi Ren, Yong-Ning Zhou, Qian Sun, Zheng-Wen Fu*

Shanghai Key laboratory of Molecular Catalysts and Innovative Materials, Department of Chemistry & Laser Chemistry Institute, Fudan University, Shanghai 200433, PR China

ARTICLE INFO

Article history:
Received 20 July 2011
Accepted 12 October 2011
Available online 17 October 2011

Keywords:
Tin phosphates
Magnetron sputtering
Thin film
Lithium-ion batteries

ABSTRACT

Amorphous $Sn_2P_2O_7$ thin film electrodes have been successfully fabricated by radio frequency (r.f.) magnetron sputtering. Reversible lithiation and delithiation processes occurring at 1.47 V and 2.01 V versus lithium are observed in both discharge/charge curves and cyclic voltammograms of the amorphous $Sn_2P_2O_7$ thin film electrodes for the first time. Large reversible capacity around 887 mAh g^{-1} is achieved when the cell is cycled between 0.01 V and 4.0 V, corresponding to 9.2 Li per $Sn_2P_2O_7$ unit. Based on X-ray diffraction (XRD), X-ray photoelectron spectroscopy (XPS), transmission electron microscopy (TEM) and selected area electron diffraction (SAED) evidences, the reaction mechanism involving the reversible decomposition and regeneration of amorphous $Sn_2P_2O_7$ as well as alloying and de-alloying of tin with lithium is proposed.

1. Introduction

In order to meet the increasing demands of the rapid development of electronic devices, Li-ion batteries with higher energy density are urgently required [1,2]. Apparently, the low theoretical capacity of commercial negative electrode material graphite (372 mAh g^{-1}) is one of the major obstacles to overcome. Up to now, tremendous attempts on searching for novel cheap and environmental friendly anode materials with large reversible capacities and good cyclic performances have been carried out [3,4]. Among these studies, metal tin draw lots of attentions due to the large capacities brought by alloying reactions involving the formation of $Li_{22}Sn_5$ phase [5,6]. However, it suffered large volume expansion–contraction during lithiation and delithiation processes, resulting in poor capacity retention. An effective way to improve this drawback is to introduce an inactive matrix, which can buffer the volume change during cycling.

Tin based alloy, tin oxide, tin nitride and tin phosphates have been widely investigated based on this consideration. Behm and Irvine [7] suggests crystalline $Sn_2P_2O_7$ as a potential anode material, because it could exhibit a reversible specific capacity above 360 mAh g^{-1} with good capacity retentions over 100 cycles. Xiao et al. [8] compared the electrochemical performance of amorphous and crystalline $Sn_2P_2O_7$ and found that they have similar capacity and fade characteristics with cycling in the potential range of 0–1.2 V vs. Li/Li^+. The reaction mechanism of $Sn_2P_2O_7$ with lithium was generally considered as follows:

$$Sn_2P_2O_7 + 4Li^+ + e^- \rightarrow 2Sn + Li_3PO_4 + LiPO_3 \quad (1)$$

$$Sn + 4.4Li \leftrightarrow Li_{4.4}Sn \quad (2)$$

Reaction (1) occurs in the initial discharge process. Lithium reacts with irreversibly to form metallic tin accompanied by the dissociation of the $P_2O_7^{4-}$ structure. The tin atoms dispersed in Li_3PO_4 and $LiPO_3$ networks are the hosts for further alloying reactions. In subsequent cycles, reaction (2) was only involved. Li_3PO_4 and $LiPO_3$ were inactive and played the role in keeping the Li–Sn particles mechanically connected during the large volume changes of the alloying reaction (Reaction (2)), which is similar as Li_2O in SnO system [9]. A mesoporous/crystalline $Sn_2P_2O_7$ were fabricated by Cho's group [10–14]. It showed superior electrochemical properties with a large initial capacity (ca.721 mAh g^{-1}) and excellent cyclability (ca. 587 mAh g^{-1} at the 30th cycle) in the voltage range of 0–2.5 V. They believed the mesoporous structure could effectively buffer the volume change during lithiation/delithiation processes. Recently, Li et al. [15] fabricated carbon-coated macroporous $Sn_2P_2O_7$ by hydrothermal synthesis. It could be cycled in a larger voltage range of 0–3 V with good reversibility.

Herein we will report the fabrication of an amorphous $Sn_2P_2O_7$ thin film by radio frequency (r.f.) magnetron sputtering as an anode material. The galvanostatic cycling and cyclic voltammetry curves which are different from those in previous reports are found when it is cycled between 0.01 and 4.0 V. A new electrochemical reaction mechanism is revealed based on X-ray diffraction (XRD), X-ray photoelectron spectroscopy (XPS), transmission electron

* Corresponding author. Tel.: +86 21 65642522; fax: +86 21 65102777.
E-mail address: zwfu@fudan.edu.cn (Z.-W. Fu).

0378-7753/$ – see front matter © 2011 Elsevier B.V. All rights reserved.
doi:10.1016/j.jpowsour.2011.10.039

microscopy (TEM) and selected-area electron diffraction (SAED) measurements.

2. Experimental

$Sn_2P_2O_7$ target with a 5 cm diameter was pressed from the $Sn_2P_2O_7$ powders (99.99%, Aldrich). The thin films were deposited directly on the stainless steel substrate by r.f. magnetron sputtering at room temperature. The background vacuum of the sputtering chamber was below 5×10^{-4} Pa, evacuating with a mechanical pump and a turbo-molecular pump. The distance between substrate and target was 5 cm while the pressure of Ar ambient gas during deposition was controlled at 1.0 Pa by a needle valve. The r.f. power was about 40 W. The deposition time was about 1.5 h after a 10 min pre-sputtering of the target to remove target contamination. The thickness of the as-deposited thin film was measured to be about 200 nm by a profilometer (Tencor Alpha-Step 200). Weight of the thin film was directly obtained by substracting the original substrate weight from the total weight of the substrate and the deposited thin film onto its surface, which were examined by an electrobalance (BP 211D, Sartorius, the precision of the weight was ±0.01 mg). It was found to be about 0.12 mg with the area of 1.0 cm^2.

For the electrochemical measurements, the cells were constructed using the as-deposited $Sn_2P_2O_7$ thin film as a working electrode and two lithium sheets as the counter and reference electrodes, respectively. The electrolyte consisted of 1 M $LiPF_6$ in a nonaqueous solution of ethylene carbonate (EC) and dimethyl carbonate (DMC) with a volume ratio of 1:1 (Merck). The cells were assembled in an Ar filled glove box. Galvanostatic cycling measurements were carried out at room temperature with a Land CT 2001A battery test system. The cells were cycled between 0.01 and 4.0 V at a current density of 5 μA cm^{-2}. CV tests were performed with a scanning rate of 0.2 mV s^{-1} on a CHI660A electrochemical working station (CHI Instruments, TN).

The XRD patterns of the thin film electrodes were recorded by a Rigata/max-C diffractometer with Cu Kα radiation. TEM and SAED measurements were carried out with a JEOL 2010 TEM at 160 kV accelerating voltage. XPS measurements were performed on a Perkin-Elmer PHI 5000C ECSA system with monochromatic Al Kα (1486.6 eV) irradiation.

For the *ex situ* measurements, to avoid the exposure to oxygen or water, the cells at different stages were dismantled in an Ar-filled glove box and the electrodes were rinsed in anhydrous DMC to eliminate residual salts. For TEM and SAED measurements, the active materials were scratched from the stainless steel substrate. The loose powders were then mixed with ethanol to prepare slurry, out of which one drop was taken, and deposited on a copper grid. To avoid exposure to oxygen or water, the grids were rapidly transferred into the chambers for cleanliness.

3. Results and discussion

The Li storage capacities and cycle performance of $Sn_2P_2O_7$ film were investigated by discharge/charge measurements. Fig. 1(a) shows the charge/discharge curves of $Sn_2P_2O_7$/Li cells cycled between 0.01 and 4.0 V at a constant current density of 5 μA cm^{-2}. The initial open-circuit voltage plateaus (OCV) of the cell is 2.86 V. Two voltage plateaus appear around 1.35 and 0.53 V in the initial discharging process, respectively, which is a typical discharge curve of $Sn_2P_2O_7$ [10]. The capacity of the initial discharge is found to be 1525 mAh g^{-1}. The second discharge/charge processes of the cell yield a reversible discharge capacity of 887 mAh g^{-1}, corresponding to 9.2 Li per $Sn_2P_2O_7$. It is much larger than the $Sn_2P_2O_7$ anode reported previously [7,8,10–15]. Beside, a slopy plateau could be

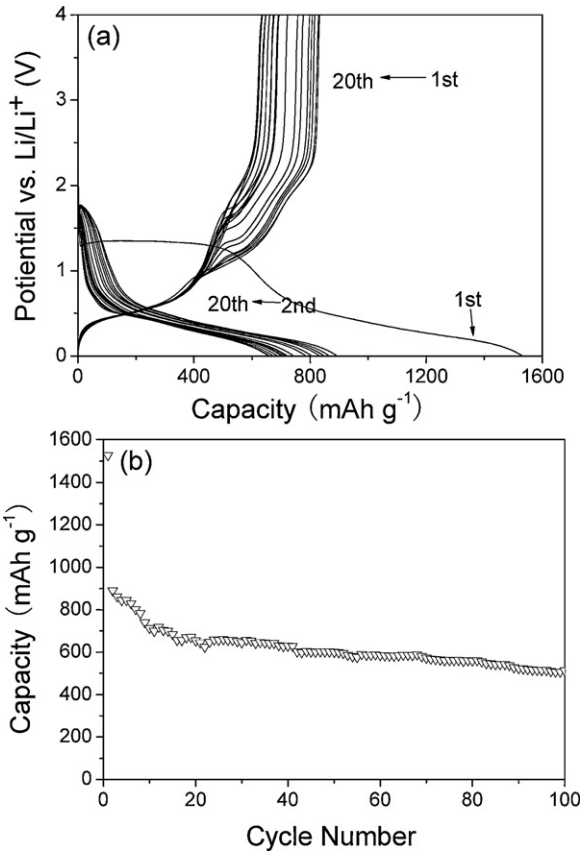

Fig. 1. (a) Voltages composition profiles for the $Sn_2P_2O_7$ thin film/$LiPF_6$/Li cells. The specific capacity was based on weight of complete thin film and (b) cycling performance of the $Sn_2P_2O_7$ thin film in 100 cycles.

observed at around 1.6 V in charging process, which was never found in previous study. It implies a new electrochemical reaction process at this potential. Fig. 1(b) shows the cycling performance of the $Sn_2P_2O_7$/Li cell at a current density of 5 μA cm^{-2} in 100 cycles. It can be seen that the capacity fading is fast in first 10 cycles. Subsequently, the capacity could be well kept. After 100 cycles, a reversible capacity of 513 mAh g^{-1} is still obtained. As discussed by Courtney and Dahn [9], the tin-based oxides are quite sensitive to the potential limits of the cycling. Too wide voltage range leads to more rapid capacity fading. In this study, the upper potential is up to 4.0 V, much higher than previous work [7,8,10–15], but the capacity fading is not that serious.

Fig. 2(a) illustrates the first three cyclic voltammorgrams (CV) of the as-deposited $Sn_2P_2O_7$ thin film electrode between 0.01 and 4.0 V measured at a scan rate of 0.2 mV s^{-1}. In the first discharging process, one narrow peak and two partially overlapped broad peaks appear at 0.95, 0.34 and 0.16 V, respectively. These potentials are lower than those in the work of Behm [7] and Xiao [8], whose initial redox peak is at 1.6 V. During the first charging process, three cathodic peaks around 2.0, 1.22 and 0.56 V imply multi-step delitiating reactions taking place. In subsequent cycles, the reduction peaks at 0.34 and 0.16 V basically sustained while the peak at 0.95 V significantly shift to higher potential of 1.5 V with sharp intensity drop. A comparison of the voltammetric features between the second and the third scan reflects the lithium insertion/extraction reactions are more reversible in thin film $Sn_2P_2O_7$ than bulk one. The CV result is in good agreement with the galvanostatic curves. To reveal the corresponding oxidation peak to reduction peak at 0.95 V, we set the potential range from 0.7 to 3.0 V at a scan rate of 0.2 mV s^{-1} (Fig. 2(b)). In the first discharge, the large reduction peak located at 0.91 V. In the first charge, we could only see the

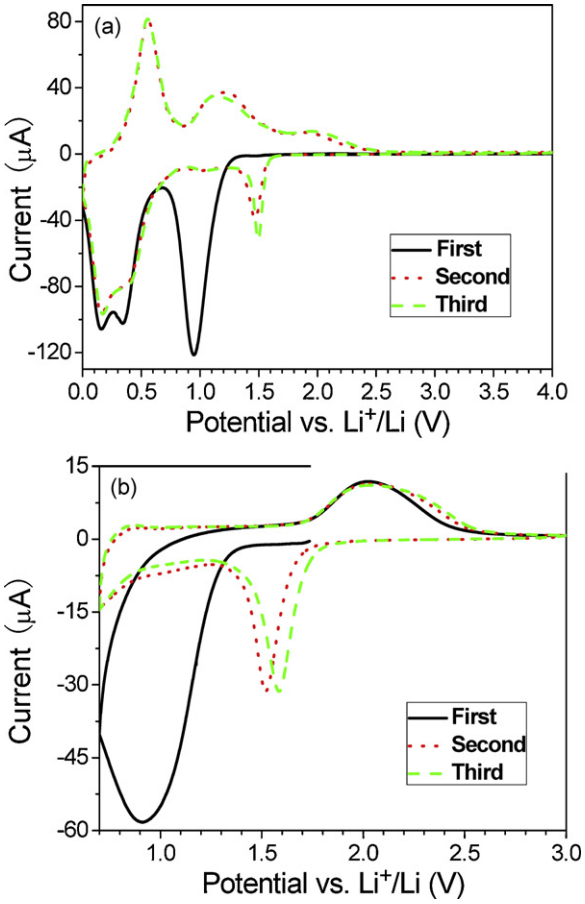

Fig. 2. The first three cyclic voltammograms for the $Sn_2P_2O_7$ thin film with a limited voltage range of (a) 0.01–4.0 V and (b) 0.7–3.0 V at a scan rate of 0.2 mV s^{-1}.

oxidation peak at 2.0 V. The peaks at 1.22 and 0.56 V in Fig. 2(a) vanish. During the subsequent Li^+ insertion/exaction processes, the reduction peak shifts to 1.5 V just like that in Fig. 2(a). Nonetheless, the anode peak at 2.0 V shifts little without any fading. In subsequent cycles, the couple of redox peaks around 2.0 and 1.5 V could be well kept with slight shift indicating good reversibility. The two peaks which are never observed in previous study [7,8,10–15] indicated new electrochemical reaction process may be involved.

To examine the structure and composition of the as-deposited, discharged and charged thin film, X-ray diffraction measurement was employed at first. However, none of diffraction peaks except those of stainless steel substrate can be observed in the XRD pattern of the as-deposited, discharged or charged thin films (not shown here). It may be due to their amorphous structure or their nano-sized particles smaller than the X-ray coherence length. Therefore, TEM and SAED measurements were carried out on these electrodes. Fig. 3(a) shows the TEM image of the as-deposited $Sn_2P_2O_7$ thin film. No crystal lattice can be observed. Corresponding SAED spectra shown in Fig. 3(b) are blurred, indicating amorphous structure of the as-deposited $Sn_2P_2O_7$. After discharging to 0.01 V, the HRTEM image of the thin film (Fig. 4(a)) shows better ordered structure with some hazy strips. The corresponding SAED pattern (Fig. 4(b)) exhibits some clear concentric rings and some bright spots, indicating the polycrystalline nature of the lithiated thin film. The measured d-spacings of 3.96 Å, 1.84 Å, and 2.73 Å, 2.35 Å derived from the SAED pattern can be well indexed to the (1 2 0), (3 1 1) planes of Li_3PO_4 (JCPDS card No. 84-0046) and (6 4 0), (8 2 2) planes of $Li_{22}Sn_5$ (JCPDS card No. 18-0753), respectively, indicating that $Sn_2P_2O_7$ is decomposed after the initial discharging process while $Li_{22}Sn_5$ and Li_3PO_4 are formed. After first charging to 4.0 V, HRTEM

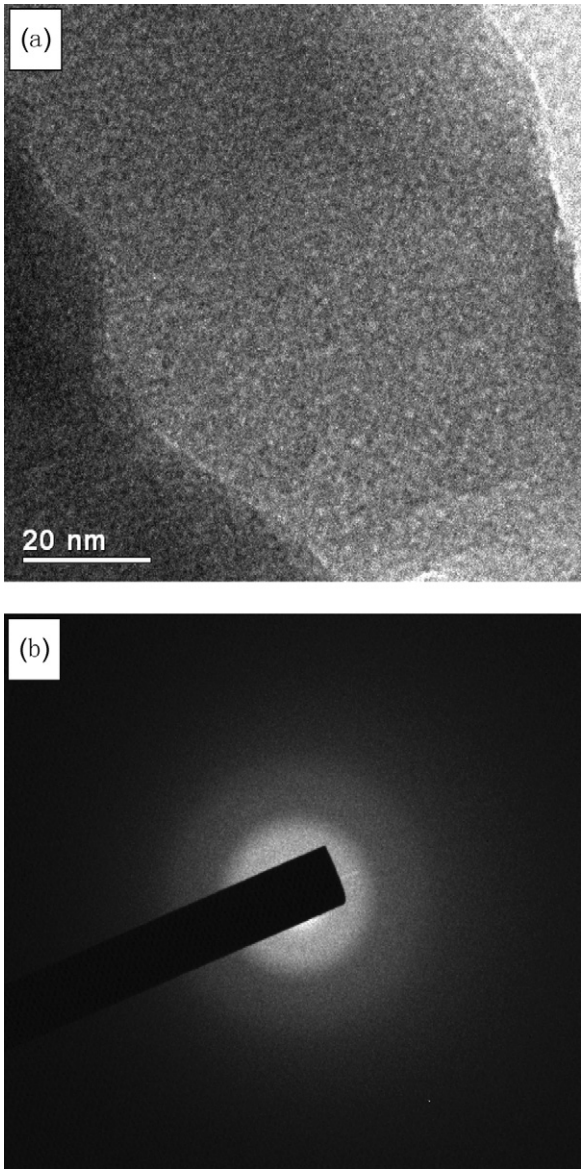

Fig. 3. (a) The TEM image and (b) SAED pattern of the as-deposited $Sn_2P_2O_7$ thin film fabricated by r.f. sputtering.

image shown in Fig. 5(a) exhibits a porous structure, which should be caused by volume contraction during the delithiation process. However, no clear lattice could be observed. Corresponding SAED patterns in this region (Fig. 5(b)) shows spread rings similar as those of the as-deposited films indicating the charging film comes back to amorphous structure.

To further confirm the discharged and charged products, XPS measurement was carried out. Fig. 6 shows the O 1s, P $2p_{3/2}$, and Sn $3d_{5/2}$ spectra of $Sn_2P_2O_7$, respectively. In these figures, curves (1) and (2) represent the electron binding energy of the stannous pyrophosphate target and the as-deposited thin film. It can be seen that the peaks of the as-deposited thin film are at the same position as the target, indicating that the as-deposited film obtained same composition as $Sn_2P_2O_7$ target. Curves (3) and (4) show the electron binding energy after discharging to 0.01 V and after charging to 4.0 V, respectively. We can clearly see that peaks of the thin film after discharging to 0.01 V are different from those of the as-deposited film. The electron binding energy of P $2p_{3/2}$ splits to two peaks at 132.1 and 134.4 eV indicates the existence of PO_4^{3-} and PO_3^-, respectively [16]. It is consistent with the TEM

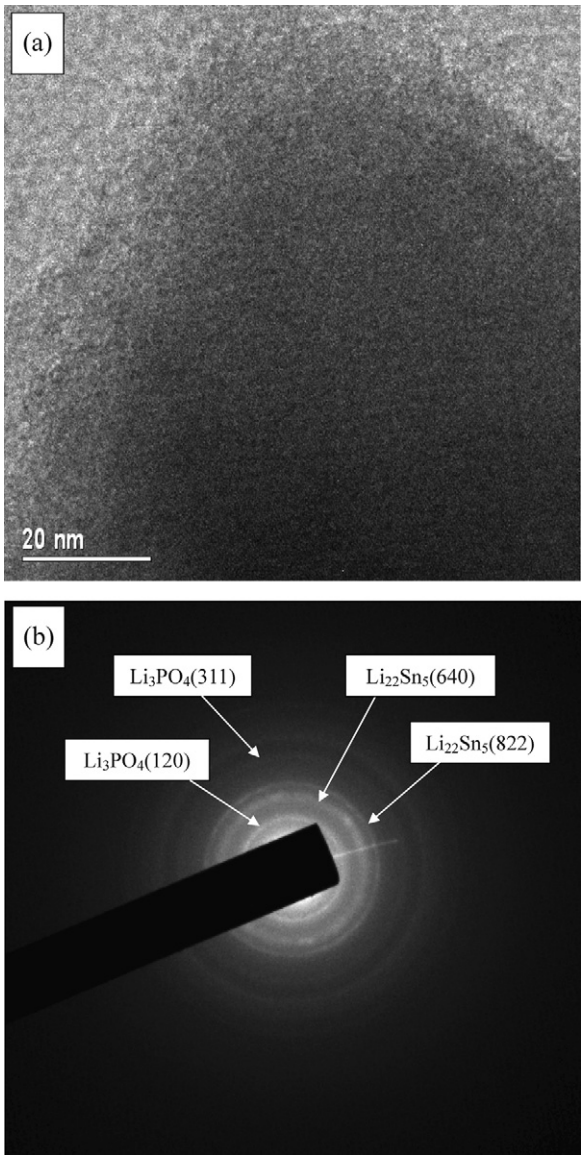

Fig. 4. (a) The *ex situ* TEM image and (b) SEAD pattern of $Sn_2P_2O_7$ thin film electrode after discharging to 0.01 V.

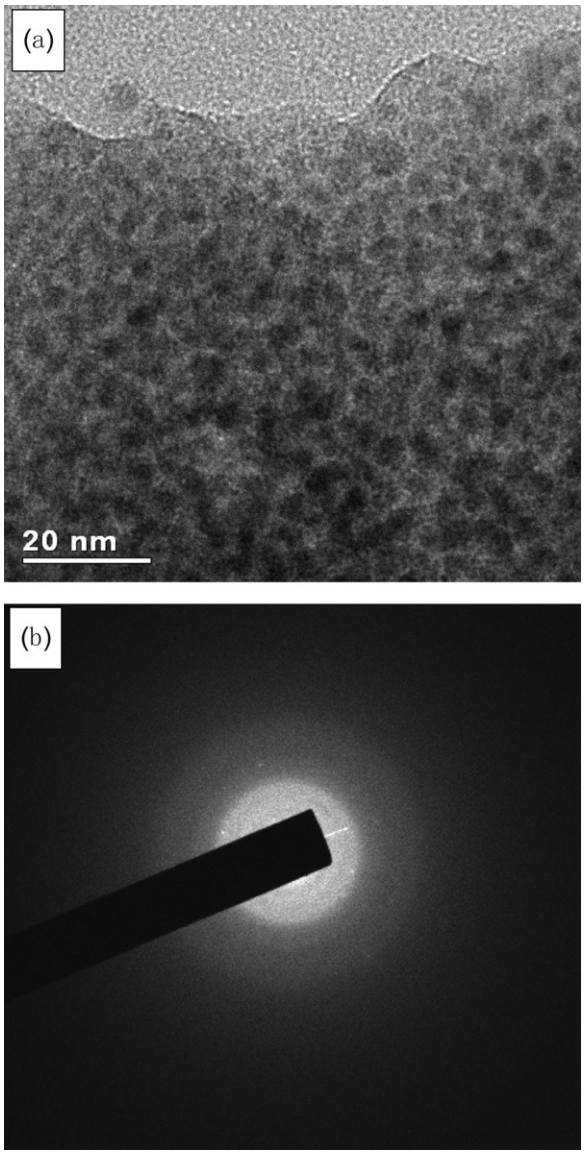

Fig. 5. (a) The *ex situ* TEM image and (b) SEAD pattern of $Sn_2P_2O_7$ thin film electrode after charging to 4.0 V.

characterization. Besides, the binding energy peak of Sn $3d_{5/2}$ shifts to lower energy by 1.4 eV. A new small peak appears at 482.9 eV. The left shifting of energy peak indicates that Sn^{2+} is reduced into metal Sn during the initial discharging process and the small peak at 482.9 eV is a typical state of tin–lithium alloy. The existence of part of metal Sn during the first discharging process suggest that Sn is not totally reacted with Li^+ because of its electrochemical inactivity [17]. After recharging to 4.0 V, the peak of O 1s, P $2p_{3/2}$ and Sn $3d_{5/2}$ shift back to the same position as the as-deposited thin film, which reflects that $Sn_2P_2O_7$ is reproduced after recharging process.

Based on above results, the electrochemical reaction mechanism of $Sn_2P_2O_7$ with lithium involving the following steps is proposed.

First discharge process:

$$Sn_2P_2O_7 + 4Li^+ + 4e^- \rightarrow 2Sn + Li_3PO_4 + LiPO_3 \quad (3)$$

$$Sn + 4.4Li^+ + 4.4e^- \rightarrow Li_{4.4}Sn \quad (4)$$

Subsequent cycles:

$$Li_{4.4}Sn \leftrightarrow Sn + 4.4Li^+ + 4.4e^- \quad (5)$$

$$Sn + Li_3PO_4 + LiPO_3 \leftrightarrow Sn_2P_2O_7 + 4Li^+ + 4e^- \quad (6)$$

These steps during the discharge and charge processes are in according with CV curves as shown in Fig. 2(a) and (b). In the first discharge, the peak at 0.95 V could be attributed to the decomposition of $Sn_2P_2O_7$ (reaction (3)). The peaks at 0.34 and 0.16 V correspond to the multi-step alloying reaction between Sn and Li (reaction (4)). In the charging process, the peak at 0.56 and 1.22 V corresponds to the dealloying reaction of $Li_{4.4}Sn$ (reaction (5)). The other peak at 2.0 V could be attributed to the reformation of $Sn_2P_2O_7$ (reaction (6)). In subsequent cycles, the redox couple of the peaks at 2.0 and 1.5 V is found for the first time and confirmed the existence of reaction (6). Recently, Guo et al. [18] have studied the electrochemical performance of Fe/Li_3PO_4 nanocomposite system, a lithium storage capacity up to 220 mAh g^{-1} was found with considerable capacity retention between 0.005 and 1.7 V. They found that the Fe and Li_3PO_4 nanograins are stable up to 4.2 V. They ascribed the reversible capacity to lithium storage on the boundaries of the Fe and Li_3PO_4 nanograins. Apparently, it is quite different from our $Sn_2P_2O_7$ thin films. In our case, it is found that Li_3PO_4 and $LiPO_3$ could be decomposed to regenerate $Sn_2P_2O_7$ under the driven of nano sized metal Sn during the charging process. This process is similar as that of SnO_2 thin film [19], which

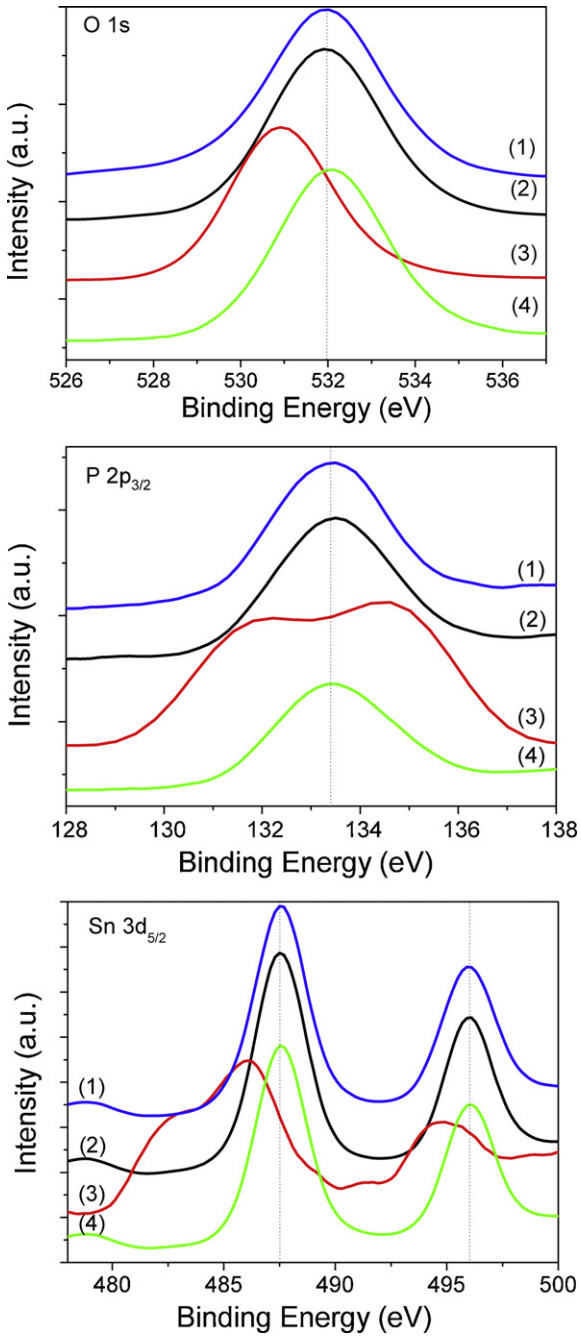

Fig. 6. O 1s, P $2p_{3/2}$ and Sn $3d_{5/2}$ XPS spectra for (1) $Sn_2P_2O_7$ powder; (2) the as-deposited thin film; (3) thin film electrode after discharging to 0.01 V; and (4) thin film electrode after charging to 4.0 V.

Sn particles could drive the decomposition of Li_2O and regenerate SnO_2. The equilibrium between the pyrophosphate anions and the products of their disproportionation could be suggested as follows [20]:

$$(PO_3)^{2-}\text{–O–}(PO_3)^{2-} \leftrightarrow (PO_4)^{3-} + \text{–O–}(PO_2)^{-} \quad (7)$$

This equilibrium provides the support for one possible reaction pathway to reaction (6), in which nano sized metal Sn could drive the decomposition of Li_3PO_4 and $LiPO_3$ with the formation of $Sn_2P_2O_7$. The formation of solid electrolyte interface (SEI) [21] on the anode surface and a changed structure of reproduced $Sn_2P_2O_7$ should be responsible for irreversible capacity in the first cycle. In subsequent cycles, the $Li_3PO_4/LiPO_3$ matrix could effectively buffer the volume change during alloying and dealloying reactions between Sn and Li at the potential below 1.0 V. Furthermore, $Li_3PO_4/LiPO_3$ could react with Sn particles to reform $Sn_2P_2O_7$ under a charging potential around 2.0 V and extract more lithium. It results in larger reversible capacities and considerable capacity retention. These results may supply new concept on the lithium electrochemical investigation of metal phosphate.

4. Conclusions

Amorphous $Sn_2P_2O_7$ thin film fabricated by radio frequency magnetron sputtering as an anode material for lithium-ion batteries was reported. Galvanostatic cycling of $Sn_2P_2O_7$ film electrode showed well capacity retention and cycle performance with a large reversible capacity around 887 mAh g^{-1}. Our results demonstrated that the reversible formation and decomposition of Li_3PO_4 and $LiPO_3$ could be driven by metal tin. Large reversible capacity of $Sn_2P_2O_7$ thin film electrode makes it one of the promise anode materials for future lithium-ion batteries. These findings provide a new possibility for further clarifying the intrinsic properties of $Sn_2P_2O_7$ electrode.

Acknowledgements

This work was financially supported by Science & Technology Commission of Shanghai Municipality (08DZ2270500 and 09JC1401300), China Postdoctoral Science Foundation (No. 20100470660) and 973 Programs (No. 2011CB933300) of China.

References

[1] J.M. Tarascon, M. Armand, Nature 414 (2001) 359–367.
[2] F. Gillot, S. Boyanov, L. Dupont, M.L. Doublet, M. Morcrette, L. Monconduit, J.M. Tarascon, Chem. Mater. 17 (2005) 6327–6337.
[3] Q. Wang, R. Gao, J.H. Li, Appl. Phys. Lett. 90 (2007), 143107(1-3).
[4] R. Demir-Cakan, Y.S. Hu, M. Antonietti, J. Maier, M.M. Titirici, Chem. Mater. 20 (2008) 1227–1229.
[5] C.C. Chang, S.J. Liu, J.J. Wu, C.H. Yang, J. Phys. Chem. C 111 (2007) 16423–16427.
[6] L. Wang, S. Kitamura, K. Obata, S. Tanase, T.J. Sakai, Power Sources 141 (2005) 286–292.
[7] M. Behm, J.T.S. Irvine, Electrochim. Acta 47 (2002) 1727–1738.
[8] Y.W. Xiao, J.Y. Lee, A.S. Yu, Z.L. Liu, J. Electrochem. Soc. 146 (1999) 3623–3629.
[9] I.A. Courtney, J.R. Dahn, J. Electrochem. Soc. 144 (1997) 2045–2052.
[10] E. Kim, D. Son, T.G. Kim, J. Cho, B. Park, K.S. Ryu, S.H. Chang, Angew. Chem. Int. Ed. 43 (2004) 5987–5990.
[11] E. Kim, M.G. Kim, Y. Kim, J. Cho, Electrochem. Solid-State Lett. 8 (2005) A452–A455.
[12] E. Kim, Y. Kim, M.G. Kim, J. Cho, Electrochem. Solid-State Lett. 9 (2006) A156–A159.
[13] E. Kim, M.G. Kim, J. Cho, Electrochem. Solid-State Lett. 9 (2006) A311–A314.
[14] H. Kim, G.S. Park, E. Kim, J. Kim, S.G. Doo, J. Cho, J. Electrochem. Soc. 153 (2006) A1633–A1636.
[15] Y.M. Li, J.H. Li, J. Phys. Chem. C 112 (2008) 14216–14219.
[16] J.F. Moulder, W.F. Stickle, P.E. Sobol, K.D. Bomben, Handbook of X-ray Photoelectron Spectroscopy, Perkin-Elmer Corp., Physical Electronics Division, Eden Prairie, MN, 1992.
[17] S. Machill, T. Shodai, Y. Sakurai, J. Yamaki, J. Solid. State. Electrochem. 3 (1999) 97–103.
[18] X.W. Guo, X.P. Fang, Y. Mao, Z.X. Wang, F. Wu, L.Q. Chen, J. Phys. Chem. C 115 (2011) 3803–3808.
[19] M.Z. Xue, Z.W. Fu, Electrochem. Solid-State Lett. 9 (2006) A468–A470.
[20] A.M. Efimov, J. Non-Cryst. Solids 209 (1997) 209–226.
[21] J.Z. Li, H. Li, Z.X. Wang, X.J. Huang, L.Q. Chen, J. power Sources 81-82 (1999) 346–351.